J Physiol 589.3 (2011) pp 609–627

The Journal of Physiology

Cholinergic modulation amplifies the intrinsic oscillatory properties of CA1 hippocampal cholecystokinin-positive interneurons

Christian A. Cea-del Rio[1], J. Josh Lawrence[1,2], Ferenc Erdelyi[3], Gabor Szabo[3] and Chris J. McBain[1]

[1] *Program in Developmental Neurobiology, Eunice Kennedy Shriver, National Institute of Child Health and Human Development, Bethesda, MA 20892, USA*

[2] *Centre for Structural and Functional Neuroscience, Department of Biomedical and Pharmaceutical Sciences, 385 Skaggs Bldg, University of Montana, Missoula, MT 59801, USA*

[3] *Laboratory of Molecular Biology and Genetics, Institute of Experimental Medicine, Hungarian Academy of Sciences, Budapest, Hungary*

Non-technical summary In the mammalian hippocampus, the neurotransmitter acetylcholine (ACh) promotes learning and memory storage. During sensory processing and learning, large ACh-dependent electrical oscillatory events are observed, which involve the synchronization of both inhibitory and excitatory neural circuits. While the actions of ACh are known on excitatory hippocampal circuits, its actions on specific inhibitory circuits are poorly understood. We show that two types of cholecystokinin-positive local circuit inhibitory interneuron, the so-called 'basket cells' and 'Schaffer collateral-associated' cells, which innervate separately the cell body and dendritic regions of principal cells, are modulated similarly by cholinergic receptor activation. In both cell types activation of their muscarinic receptors triggers a general increase of excitability and intrinsic oscillatory activity, and a more efficient engagement to slow network oscillations. Knowledge of how cholinergic neuromodulation acts on neurochemically identical but morphologically distinct inhibitory interneurons will allow us to understand the role played by this important neuromodulator during hippocampal-dependent tasks *in vivo*.

Abstract Cholecystokinin (CCK)-containing interneuron subpopulations provide GABAergic inhibition to multiple surface domains of CA1 hippocampal pyramidal cells. CCK-basket cells (BCs) control AP initiation through perisomatic inhibition, whereas dendritically projecting Schaffer collateral-associated (SCAs) cells probably shape dendritic excitability and synaptic integration. We have shown previously that muscarinic receptor (mAChR) activation regulates firing properties and excitability of CCK-BCs; however, little is known about mAChR modulation of the related but anatomically distinct CCK-SCA population. Here, using whole-cell recordings and single-cell RT-PCR, we show that muscarine elicited a biphasic hyperpolarizing–depolarizing voltage response in CCK-SCAs, which was mediated by opposing actions of M1 and M3 mAChRs, respectively. In addition, like CCK-BCs, CCK-SCAs exhibited an M3-mediated increase in AP firing frequency and an afterdepolarization mediated synergistically by both M1 and M3 mAChRs. Spontaneous M3-mediated membrane potential oscillations (1–2 Hz) were observed in both CCK-SCAs and CCK-BCs. Using sinusoidal current injection we examined how mAChR activation of CCK interneurons alters intrinsic oscillatory properties and AP frequency preference. In CCK-BCs and CCK-SCAs, APs occurred preferentially at delta/theta frequencies (1–7 Hz) under control conditions. mAChR activation extended the AP phase-locking bandwidth into the theta and beta frequency range for CCK-SCAs and CCK-BCs respectively. This was accompanied by changes in both AP phase and precision. In conclusion, anatomically distinct CCK+ cells show similar changes in excitability, firing pattern activity and oscillatory preferences

DOI: 10.1113/jphysiol.2010.199422

during cholinergic modulation suggesting that CCK+ interneurons probably act cooperatively to collectively synchronize the hippocampal network along the somatodendritic axis of the CA1 pyramidal cells during muscarinic receptor activation.

(Received 11 September 2010; accepted after revision 29 November 2010; first published online 29 November 2010)
Corresponding author C. J. McBain: Porter Neuroscience Center, Bldg 35, Rm 3C903, 35 Lincoln Drive, Bethesda, MD 20892, USA. Email: mcbainc@mail.nih.gov

Abbreviations ADF, afterdeflection; ADP, afterdepolarization; AHP, afterhyperpolarization; AP, action potential; BCs, basket cells; CB, calbindin; CB1-R, cannabinoid receptor type 1; CCK, cholecystokinin; DSI, depolarization-induced suppression; HW, half width; mAChR, muscarinic acetylcholine receptor; MPO, membrane potential oscillation; MS-DBB, medial septum-diagonal band of Broca; O-LM, oriens-lacunosum moleculare; PV, parvalbumin; R, rotation number; SCAs, Schaffer collateral-associated cells; scRT-PCR, single-cell RT-PCR.

Introduction

The hippocampus contains a neurochemically and morphologically diverse population of local circuit inhibitory interneurons whose physiological properties (Freund & Buzsaki, 1996; Ascoli *et al.* 2008), activity during network behaviour (Klausberger & Somogyi, 2008) and capacity for neuromodulation (Bergles *et al.* 1996; Gulyas *et al.* 1999*a*; Lawrence, 2008) are being increasingly better defined. Within the CA1 hippocampus two major cholecystokinin (CCK)-containing interneuron populations are found. CCK-basket cells (CCK-BCs) innervate the perisomatic and proximal dendrites of pyramidal cells (Foldy *et al.* 2010) and CCK-Schaffer collateral-associated cells (CCK-SCAs) which target pyramidal cell dendrites. Both cell types share common passive and active electrophysiological properties, possessing similar membrane time constants, spike firing accommodation and AP amplitude (Cope *et al.* 2002; Lee *et al.* 2010). CCK+ interneurons recorded *in vivo* present AP firing locked to the ascending phase of theta oscillations (Klausberger *et al.* 2005). Additionally, CCK+ cells often co-express calbindin (CB) (Kubota & Kawaguchi, 1997; Cope *et al.* 2002; Cea-del Rio *et al.* 2010) and the endocannabinoid receptor type 1 (CB1-R) on their presynaptic terminals and are major targets for numerous modulatory agents (Katona *et al.* 1999).

Given these properties CCK+ interneurons probably play several distinct functionally important roles in the hippocampus. The long membrane time constant (~25 ms) of CCK-BCs makes them particularly suited for the integration of excitation from multiple afferents during a temporal window wider than other perisomatic innervating interneurons (Glickfeld & Scanziani, 2006). Postsynaptically, CCK-BCs control pyramidal cell excitability by regulating Na^+-dependent AP initiation (Freund & Katona, 2007), thus modulating and synchronizing large groups of pyramidal cells. In contrast, CCK-SCAs somata and dendrites are primarily aligned with the Schaffer collateral/commissural input into the stratum radiatum (Hajos & Mody, 1997; Gulyas *et al.* 1999*b*; Cope *et al.* 2002), allowing them to participate in feed-forward inhibitory control of CA1 pyramidal cell apical dendrites (Pouille & Scanziani, 2001). Their dendritic targeting axons probably regulate local dendritic integration and Ca^{2+}-dependent spike initiation and/or propagation (Miles *et al.* 1996).

Numerous studies have examined cholinergic neuromodulation of morphologically defined CA1 hippocampal interneurons (Parra *et al.* 1998; McQuiston & Madison, 1999; Widmer *et al.* 2006). Recent studies have shown specific and differential pre- and postsynaptic cholinergic phenotypes in neurochemically and morphologically identified PV-BCs, PV-axo-axonic cells, O-LM cells and CCK-BCs (Lawrence *et al.* 2006*b*; Cea-del Rio *et al.* 2010; Szabo *et al.* 2010). In CCK-BCs, both endogenous acetylcholine release and application of muscarinic receptor agonists elicit a postsynaptic increase in firing activity concomitant with a pronounced spike afterdepolarization (Cea-del Rio *et al.* 2010). How muscarinic receptor activation modulates the neurochemically related but anatomically distinct CCK-SCAs is unclear. However, mAChR activation of stratum radiatum interneurons of unknown neurochemical origin (which probably included CCK-SCAs) triggers either hyperpolarization or biphasic voltage responses (McQuiston & Madison, 1999). Furthermore, Widmer *et al.* (2006) demonstrated that endogenous ACh release elicited a hyperpolarization, depolarization, oscillatory or biphasic response in neurochemically unidentified stratum radiatum interneurons (Widmer *et al.* 2006). Thus, the functional consequence of mAChR activation on unequivocally identified CCK-SCAs has not been systematically examined.

We have previously shown that identified CCK-BCs respond to mAChR activation in a stereotypic manner (Cea-del Rio *et al.* 2010). We now extend this study to question whether neurochemically similar (CCK+) but anatomically distinct cell types (BCs *versus* SCAs) respond in a similarly homogeneous manner to mAChR activation. This offers a unique opportunity to understand how cholinergic modulation affects neurochemically defined interneuron subtypes that target different somatodendritic domains of principal cells.

Using whole-cell recordings in hippocampal slices from GAD65-GFP transgenic mice to facilitate the systematic examination of CCK+ cells we now show that mAChR activation triggers increases in firing activity, AP width and the appearance of an ADP in CCK-SCAs similar to that observed in CCK-BCs. These responses are mediated through M1 and M3 mAChRs and are coupled to a biphasic hyperpolarizing–depolarizing change in membrane potential (V_m) not observed in CCK-BCs (Cea-del Rio *et al.* 2010). Both cell types possess an M3-mediated amplification of subthreshold membrane oscillatory activity in the delta frequency range (1–2 Hz). Finally, both BCs and SCAs exhibited similar AP frequency preferences, and mAChR activation increased the number and phase of spikes per oscillatory cycle. These observations demonstrate that CCK+ dendritic- and perisomatic-targeting interneurons share similar response profiles to mAChR activation, suggesting that CCK+ interneurons may act in a concerted manner to control pyramidal cell excitability.

Methods

Animals

All experiments were conducted in accordance with animal protocols approved by the National Institutes of Child Health and Human Development Animal Care and Users Committee. These experiments also comply with *The Journal of Physiology* policy and UK regulations on animal experimentation described by Drummond, 2009. In this study, transgenic GAD65-GFP animals were used due to the strategic advantage they offer in allowing identification of two morphologically distinct CCK-expressing interneurons, CCK-SCAs and CCK-BCs. The 'GAD65-GFP' mice are a heterozygous transgenic mouse line bred on a C57/Bl6 background used from line GAD65_3e/gfp5.5 30 (Lopez-Bendito *et al.* 2004). In this mouse line, a 6.5 kb segment of the GAD65 gene (that includes 5.5 kb of the 5′-upstream region, the first two exons and a portion of the third exon and the introns inbetween) drives green fluorescent protein (GFP) expression in several GABAergic neuron subpopulations.

For a number of experiments, GAD65-GFP animals were crossed with different mAChR knock-out (KO) animals to obtain GFP+ phenotypes in M1, M3 and M1/M3 mAChR KO mice. The animals obtained from these crosses were tested through genotyping protocols (tail snips). Tail snips were digested overnight at 55°C in a 2% proteinase K-lysis buffer, pH 8.5. The final concentration of the PCR reaction was 2–3 ng μl^{-1} of DNA sample, 1× PCR buffer, 0.25 mM dNTPs (each), 5% DMSO, 0.0625 U μl^{-1} AmpliTag Gold and 2.5 ng μl^{-1} of each primer. The primers used (see Supplemental Table S2 for primer sequences) were M1S1–M1A1 and M3A3, M3B for M1 (197 bp) and M3 (226 bp) mAChR wild type, respectively. The primers used to genotype mAChR knock-out mice were NEO1–M1A1 for M1 (320 bp) and M3NEO9–M3B for M3 (170 bp). Each individual PCR reaction was run on a 2% agarose gel Trackit 100 bp DNA ladder (Invitrogen, Carlsbad, CA, USA), as molecular weight marker and stained with ethidium bromide. Gel visualization was made through a DOC-PRINT-HOOD transilluminator–UV camera set (Vilber Lourmat, BP 66-Torcy Z.I. Sud, France). Only homozygous KO GFP+ animals were used in this study.

Slice preparation and solutions

Transverse acute hippocampal slices (300 μm thick) were prepared using a Vibratome 3000 deluxe (Vibratome, St Louis, MO, USA). Slices were obtained from 15- to 20-day-old mice in which GFP is expressed in GAD65-labelled CA1 hippocampal interneuron populations (Lopez-Bendito *et al.* 2004). Mice were anaesthetized by isoflurane inhalation (1–2 ml in a holding chamber) and then decapitated. The dissection solution contained (in mM): 87 NaCl, 65 sucrose, 2.5 KCl, 1.25 NaH_2PO_4, 25 $NaHCO_3$, 7 $MgCl_2$, 0.5 $CaCl_2$ and 25 glucose (equilibrated with 95% O_2 and 5% CO_2). Slices were placed in an incubation chamber at 36°C for at least 30 min before being placed in a submerged bath chamber at 30–36°C and continuously superfused at 1–2 ml min^{-1} under carbogen pressure. The extracellular solution (ECS) contained (in mM): 130 NaCl, 3.5 KCl, 1.25 NaH_2PO_4, 25 $NaHCO_3$, 2 $MgCl_2$, 2 $CaCl_2$ and 10 glucose saturated with 95% O_2 and 5% CO_2. The ECS also contained 100 μM DL-APV, 25 μM DNQX and 5 μM gabazine to block NMDA, AMPA/kainate and $GABA_A$ receptors, respectively.

Electrophysiology

GFP-labelled inhibitory interneurons were visually identified using combined differential interference contrast (DIC) and fluorescence videomicroscopy on an Olympus BX51WI microscope. Whole-cell current-clamp data were recorded with a Multiclamp 700A amplifier (Molecular Devices Corp., Union City, CA, USA), using recording pipettes (3–5 MΩ) pulled on a P97 horizontal puller (Sutter Instruments, Novato, CA. USA), and filled with intracellular solution containing (in mM): 135 potassium gluconate, 20 KCl, 10 Hepes, 0.1 EGTA, 2 MgATP and 0.3 Na_2GTP. Recordings were low-pass filtered at 4 kHz (Bessel filter) and digitized at 10 kHz (Digidata 1322A and pClamp 9.2, Molecular Devices Corp.). Bridge balance was employed throughout the current-clamp experiments.

Sinusoidal current injection

Input current protocols and analysis programs were written in Axograph X (Molecular Devices). First a 'zap function' protocol, which is a sinusoidal function delivered across a broad frequency (1 to 30 Hz) and amplitude range (60–210 pA), was applied to the recorded cells in order to determine their AP firing engagement to different frequency values. Sinusoidal current stimulation has several advantages over synaptically evoked oscillatory input in that it allows fine control over the amplitude, frequency and regularity of the input current, as well as allowing control of the initial V_m of the cell (Garcia-Munoz *et al.* 1993; Leung & Yu, 1998; Pike *et al.* 2000). Second, a 6 s sinusoidal current injection of different amplitude (multistep) but to a selected frequency value (30 pA step current injection peak to peak from 60 to 210 pA at a fixed frequency of 10 Hz) in CCK-SCAs and CCK-BCs was applied to determine the threshold for AP firing. Finally, sinusoidal current injection of amplitude determined by the sinusoidal multipstep protocol was applied to the recorded cells and repeated 3 times in each condition (1, 3, 5, 7, 10, 15, 20, 30, 50, 70 and 100 Hz in control and muscarine conditions). The starting voltage was −60 mV and noted as V_{hold}, and the bias current was adjusted throughout the experiment such that the cell was maintained at V_{hold} at the beginning of all trials in all conditions.

Both rotation number (R), defined as the average number of APs per cycle, and failure probability, defined by the failure to fire an AP on any cycle across the total number of cycles at a specific frequency, were analysed to determine the engagement frequency preferences of AP firing of CCK+ populations.

Extracellular stimulation of cholinergic afferents

Similar to Cobb and colleagues (Widmer *et al.* 2006), bipolar stimulating electrodes were fabricated from twisted Formvar-insulated nickel/chromium wire (26 μm diameter, A-M Systems, Inc.). Stimulation electrodes connected to an A360 stimulation isolator (World Precision Instruments) were placed in the CA1 stratum oriens (SO); stimuli consisted of trains of five square-wave pulses (100–600 μA fixed current intensity, 200 μs duration) at 20 Hz delivered every 5 min. The metabotropic glutamate receptor antagonist MCPG (500 μM), the $GABA_B$ antagonist CGP55845 (1 μM; Tocris Bioscience) and the cholinesterase inhibitor tacrine hydrochloride (20 μM; Tocris Bioscience) were added to the ECS as described in the text.

Morphological identification

Biocytin (0.2–0.4%) was included in the recording pipette for *post hoc* morphological identification of each recorded cell. Cells were labelled using streptavidin-conjugated Alexa Fluor 555 (Molecular Probes, Eugene, OR USA) at 1:1000 dilution (original stock 2 mg ml^{-1}; final concentration was 2 μg ml^{-1}) and imaged with a Zeiss Live DuoScan confocal microscope with a 63× objective. For every cell, confocal z stacks (0.5–1.0 μm increment, 40–60 μm total depth) of 5×5 or 7×7 ~150 μm tiles were obtained using the Multitime module of the LSM software and stitched together automatically at the completion of acquisition. Confocal images of interneurons were flat projected in Photoshop 9.0 and reconstructed using Neurolucida (MicroBrightField) for display.

Single-cell RT-PCR

After no more than 10 min of whole-cell recording, the cytoplasm was harvested via aspiration into the recording pipette. The pipette was then withdrawn to form an outside-out patch, pipette solution was expelled into a test tube (final volume of ~10 μl), and reverse transcription (RT) was performed as previously described (Lambolez *et al.* 1992). Two steps of multiplex polymerase chain reaction (PCR) were performed as previously described (Cauli *et al.* 1997). The cDNA products in the RT reaction from the cytoplasm harvested from CCK-SCAs and CCK-BCs were first amplified simultaneously using all the primer pairs (for each primer pair, the sense and antisense primers were positioned on 2 different exons). Second rounds of PCR were performed using the first PCR product as template. In this second round, each cDNA was individually amplified using its specific primer pair: GAD67, GAD65, CR, PV, CB, SOM, NPY, VIP and CCK. Primers for the vesicular glutamate transporter 1 (vGlut1) and the somatostatin intronic region (SSint) were included as controls for pyramidal cell and genomic DNA contamination, respectively (see Supplemental Table 1S for primer sequences). Cells that were positive for vGlut1 or SSint were not considered in this study. In a subset of cells, M1–M5 ACh receptor mRNAs were also probed. Each individual PCR reaction was run on a 2% agarose gel using phix174 digested by Hae III as molecular weight marker and stained with ethidium bromide.

In the sinusoidal current injection experiments scRT-PCR could not be performed because the long duration of this protocol hinders the ability to reliably harvest the cytoplasm of these cells.

Data analysis

Electrophysiological data were analysed using Axograph X software. Input resistance (R_m) for each cell was calculated from the peak of the voltage deflection average in response to a 1 s −30 pA current step. Interval inter-spike

(ISI) values were obtained using the 'event detector' code of Axograph X. The adaptation coefficient was calculated using the first ISI divided by the average of the last two ISIs of the AP train. The term after-deflection (ADF) refers to the voltage deflection at the offset of the current step injection. The ADF can be negative (afterhyperpolarization or AHP) or positive (afterdepolarization or ADP). ADF values were calculated from a 100-ms-long voltage trace average, commencing 200 ms (whole-cell experiments) or 500 ms (synaptic stimulation experiments) after the current step offset and subtracting the pre-step current-injection voltage average (holding potential). Discharge frequency values were obtained by calculating the number of APs during a 1 s step current stimulation. Power spectrum analysis of subthreshold oscillations were obtained from population averages of 5 s V_m traces at a holding potential of –60 mV and filtered between 0.8 to 100 Hz. Finally, average values in the text and figures are expressed as mean ± S.E.M. We used paired and unpaired Student's *t* tests for statistical comparisons unless otherwise stated.

Results

Physiological and neurochemical features of dendrite-targeting CCK-SCAs

We have previously described the physiological changes in passive and active properties that CCK-BCs undergo following mAChR activation, which include a prominent increase in firing frequency, accommodation, V_m depolarization and the conversion from a spike after-hyperpolarization to an afterdepolarization in response to suprathreshold current steps (Cea-del Rio *et al.* 2010). To examine whether these mAChR-induced changes in excitability are properties shared across CCK+ interneuron populations, we took advantage of GAD65-GFP transgenic mice described previously (Lopez-Bendito *et al.* 2004).

In stratum radiatum of CA1 and CA3, GAD65-GFP+ interneurons comprised both perisomatically and dendritically projecting cell types, many of which are CCK+ (Daw *et al.* 2010). In this study, we identified 35 GAD65-GFP cells with a regular adaptive spiking phenotype (Fig. 1*A* and *B*), with an AP frequency discharge similar to CCK-BCs, but higher input resistance and longer half width (HW) than CCK-BCs (Table 1). Morphological recovery of these cells revealed cells with dendrites ramifying throughout the stratum radiatum and axonal arborizations which concentrated mainly in the stratum radiatum with minor arborization in the stratum oriens (Fig. 1*C*), consistent with Schaeffer collateral-associated cells (SCAs) described previously (Vida *et al.* 1998; Daw *et al.* 2009).

To examine the neurochemical identity of these dendritically projecting, regular-spiking cells, we performed single-cell PCR in 13 of these cells (Fig. 1*D*). We examined 9 different neurochemical interneuron markers, which included GAD65, GAD67, calcium binding proteins (PV, calbindin (CB), and calretinin (CR)), and neuropeptides (neuropeptide Y (NPY), SOM, CCK and vasoactive intestinal peptide (VIP)). Consistent with their anatomical identity as SCA cells, CCK mRNA was present in 13/13 of these cells (Cope *et al.* 2002). In addition, 13/13 cells expressed GAD65 mRNA, indicative of their GABAergic phenotype (Fig. 1*D*).

To examine whether CCK-SCAs physiologically differed from CCK-BCs, we compared both passive and active properties of CCK-SCAs with the data from CCK-BCs we reported previously (Cea-del Rio *et al.* 2010). Input resistances were higher in CCK-SCAs (220 ± 9 MΩ, $n = 21$) compared to CCK-BCs (174 ± 17 MΩ, $n = 23$; unpaired *t* test $P = 0.01$; Table 1), consistent with previous reports (Cope *et al.* 2002); AP HW in CCK-SCAs (1.10 ± 0.08 ms, $n = 19$; Fig. 1*B*. Table 1) was also significantly broader than CCK-BCs (0.85 ± 0.09 ms, $n = 16$, $P = 0.04$; Table 1). CCK-SCAs showed a greater spike adaptation coefficient than CCK-BCs following larger electrotonic current steps (Fig 1*E*; CCK-SCAs, 300 pA current step: 0.36 ± 0.04, $n = 18$ *versus* CCK-BCs, 300 pA current step: 0.24 ± 0.03, $n = 16$). CCK-SCAs also exhibited higher AP firing frequencies at lower current steps (100 pA: 10.7 ± 2.0 Hz) than CCK-BCs (100 pA: 3.6 ± 1.1 Hz, $n = 16$, $P = 0.0045$), probably reflecting the higher input resistance of CCK-SCAs. AP frequency accommodation tended to limit the maximal AP firing frequency in both cell types (500 pA: CCK-SCAs: 52.3 ± 3.7 Hz, $n = 19$ *versus* CCK-BCs: 47.7 ± 4.4 Hz, $n = 16$, $P = 0.42$, Fig. 1*F*). In summary, CCK-SCAs possess passive and active properties that differ from CCK-BCs.

AP firing preferences of CCK-BCs and CCK-SCAs upon oscillatory input

Extracellular recordings from the hippocampal network reveal oscillations which appear sinusoidal and occur at several distinct frequencies superimposed on each other (Bragin *et al.* 1995). Injection of sinusoidal currents at differing frequencies has revealed that morphologically distinct interneurons present differential engagement preferences for gamma and theta activity, respectively (Pike *et al.* 2000). In order to determine the firing frequency preferences of CCK-positive interneuronal populations, we introduced sinusoidal current injection through the recording electrode at different frequencies and examined the capacity of both CCK-SCAs and CCK-BCs to elicit APs. First, to determine the threshold of

AP firing of both CCK-SCAs and CCK-BCs, a sinusoidal current injection protocol consisting of a 'zap function' was applied (see Methods for details). This protocol varies frequency linearly from 1–30 Hz and was repeated at current amplitudes between 60 and 210 pA in 30 pA increments. Supplemental Fig. S1 illustrates that although SCAs and BCs had distinct input resistances, the output properties of these cells were not significantly different when sinusoidal current injections were applied between 1 and 30 Hz at amplitudes of 120–150 pA (Supplemental Fig. S1). The AP phase-locking of CCK+ cells will be determined by their intrinsic oscillatory properties which are dependent in turn on their active conductances and RC filtering characteristics. Representative responses to sinusoidal current stimulation at 1, 5 and 20 Hz show that both CCK-SCA (Fig. 2*A*) and CCK-BC (Fig. 2*B*) fire several APs per cycle at low frequencies (Fig. 2*C* and *D*). Individual representative APs elicited per cycle

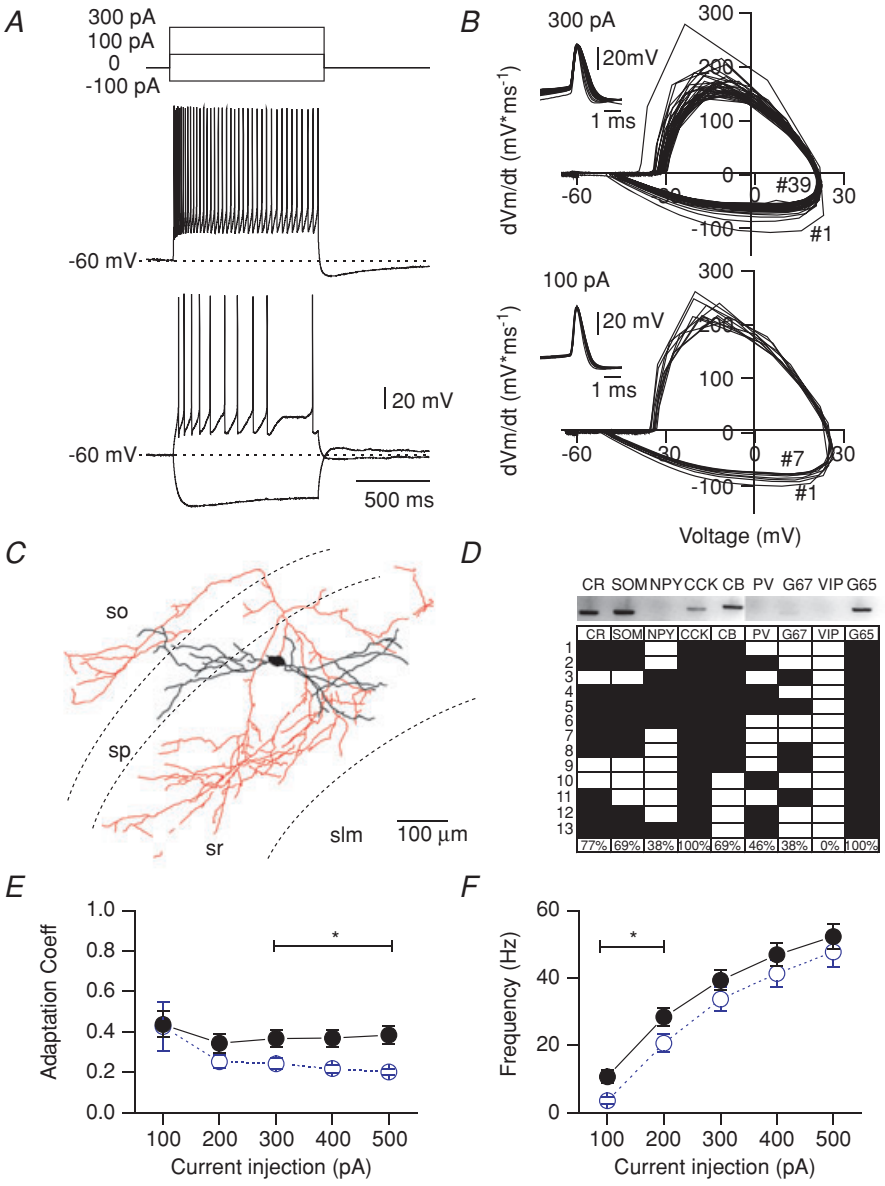

Figure 1. Electrophysiological and neurochemical properties of CCK-SCAs
A, electrophysiological properties of CCK-SCAs indicated by firing phenotype. Dotted lines indicate a V_m of –60 mV. *B*, phase plot corresponding to 100 and 300 pA representative traces and APs waveform collected in insets *C*, representative morphology of the CCK-SCAs population. *D*, representative scRT-PCR gel and neurochemical profile of a subgroup of CCK-SCAs ($n = 13$). *E*, adaptation coefficient (first inter-spike interval (ISI) divided by the average of the last two ISIs for CCK-SCAs (black circles) and CCK-BCs (blue open circles; data replotted from Cea-Del Rio *et al.* 2010), and (*F*) input–output relationship for CCK-SCAs (black circles) and CCK-BCs (blue open circles; data replotted from Cea-Del Rio *et al.* 2010).

Table 1. Passive and active electrophysiological properties of interneuron populations

	R_m (MΩ)	τ (ms)	Cm (pF)	HW (ms)	AHP (mV)	Frequency max (Hz)
CCK-SCAs	220 ± 9	42.6 ± 1.9	196 ± 12	1.1 ± 0.08	−1.8 ± 0.3	52 ± 4
CCK-BCs	174 ± 17*	40.8 ± 1.6	279 ± 25*	0.8 ± 0.09*	−1.4 ± 0.3	47 ± 4
CCK(−) R-p	238 ± 44	28.3 ± 2.6*	131 ± 22*	0.9 ± 0.06	−2.3 ± 0.6	40 ± 14
PV-BCs	76 ± 13*	31.1 ± 1.5*	592 ± 99*	0.4 ± 0.03*	−0.2 ± 0.2*	102 ± 9*

Data are expressed in mean ± S.E.M. Significant different from the CCK-SCA population are indicated by * (Student's *t* test $P < 0.05$). R_m,. input resistance; Cm = membrane capacitance; CCK(-) R-p = CCK lacking, radiatum projecting cells.

(rotation number, R) from CCK-SCAs and CCK-BCs are presented in Fig. 2*E*; in these examples both cells showed 'phase locking' (1 spike per cycle) at 5 and 7 Hz. Under control conditions, both CCK-SCAs and CCK-BCs average populations presented 'phase locking' (R = 1) at 5 Hz (Fig. 2*F*; SCAs: 1.2 ± 0.8, $n = 5$; BCs: 1 ± 0.01, $n = 3$) showing no significant differences between populations ($P = 0.63$).

These data suggest that both CCK-SCAs and CCK-BCs exhibit similar firing frequency preference and are tuned to respond to oscillatory input at 1–5 Hz.

CCK-SCAs exhibit a mAChR-induced ADP associated with a biphasic V_m change

To examine how mAChR activation alters the cellular excitability of SCAs, we applied a 1-s-long depolarizing current step from –60 mV (20 s ISI) and then, after a minute of recording, we applied muscarine (10 μM). Under control conditions CCK-SCAs exhibited accommodating AP trains to depolarizing current steps (100 pA, 1 s; Fig. 3*A*, black). Muscarine increased AP firing and triggered the appearance of an ADP (inset) at the offset of the step current injection (Fig. 3*A*, red traces). As a population, mAChR activation increased AP frequency in CCK-SCAs (from 12.7 ± 1.7 to 32.0 ± 1.9 Hz, $n = 21$, $P = 6.3 \times 10^{-9}$). When normalized to the firing frequency in control conditions, CCK-SCAs exhibited a 5.3 ± 1.7-fold higher AP frequency upon mAChR activation (Fig 3*B*). The mAChR-induced increase in firing frequency in SCAs was also associated with a shift towards regular spiking, as revealed by the change in adaptation coefficient (Fig. 3*C*; from 0.45 ± 0.08 to 0.79 ± 0.13, $P = 6.4 \times 10^{-5}$, $n = 19$). In CCK-SCAs, mAChR activation also transformed the AHP following the 1 s current step (−2.2 ± 0.2 mV) into an ADP (3.1 ± 1.2 mV, $P = 7.2 \times 10^{-5}$, $n = 21$; Fig. 3*D*).

Most striking, CCK-SCAs showed a biphasic change in V_m, in response to muscarine application (McQuiston & Madison, 1999), as revealed by the bias current required to maintain cell holding potential at –60 mV (Fig. 3*E*). CCK-SCAs require positive bias current in the first minute of the muscarine application (from −19 ± 5 pA to −11 ± 5 pA, $n = 21$, $P = 0.04$) and negative bias currents in the later 3 min compared to control conditions (from −19 ± 5 pA to −35 ± 7 pA, $n = 17$, $P = 0.003$).

We next determined whether the AP waveform of CCK-SCAs was altered by mAChR activation (Fig. 3*F* and *G*). First, under control conditions, the AP waveform in CCK-SCAs broadened when comparing the first *versus* the last 100 ms of the current step (from 0.94 ± 0.07 ms to 1.19 ± 0.09 ms, $n = 19$, $P = 1.55 \times 10^{-7}$; Fig. 3*G*, black). Under mAChR activation, the AP HW of CCK-SCAs was significantly broadened, suggesting that the conductances associated with the AP waveform are modified by mAChR activation (from 1.1 ± 0.08 ms in the first 100 ms to 1.3 ± 0.11 ms in the last 100 ms, $n = 19$, $P = 0.02$).

To determine whether the cholinergic phenotype of CCK-SCAs is related to their neurochemical or morphological identity, we studied five other cells that were neither CCK-SCA nor CCK-BCs; these cells were categorized as CCK-lacking radiatum-projecting cells (Table 1; Supplemental Fig. S2). Although CCK-lacking radiatum projecting interneurons present similar morphological characteristics as CCK-SCAs, they lacked CCK mRNA expression. In this subgroup, muscarine elicited only a subtle membrane depolarization as revealed by the negative current needed to maintain the V_m at –60 mV (−36.2 ± 7.3 pA, $n = 5$, $P = 0.03$). Similarly, muscarine triggered only a small reduction in the AHP (from −2.1 ± 0.4 mV to −1 ± 0.4 mV, $n = 5$, $P = 0.04$), and failed to significantly increase either firing frequency (2.4 ± 0.9-fold, $n = 5$, $P = 0.17$) or alter AP HW (from 0.9 ± 0.1 ms to 1.0 ± 0.1, $n = 5$, $P = 0.18$; Supplemental Fig. S2), suggesting that muscarinic receptor activation does not trigger a common phenotype across distinct stratum radiatum dendritic targeting interneurons.

In our previous study (Cea-del Rio *et al.* 2010) we demonstrated that cholinergic fibres, as revealed by vesicular ACh transporter (vAChT) immunohistochemistry, were located throughout the pyramidal cell layer proximal to both PV and CCK-basket cell types. Furthermore, synaptically released acetylcholine was shown to recapitulate the response exogenous muscarine application triggered in CCK-BCs. Here, using

a similar approach to that described in Cea-del Rio *et al.* (2010), we now show that cholinergic fibres as revealed by vAChT immunohistochemistry are also found throughout the stratum radiatum and in the local vicinity of CCK SCAs (Supplemental Fig. S4*A*). Furthermore, cholinergic fibre stimulation in the hippocampus evoked an increase in firing activity (from 9.0 ± 1.7 Hz to 18.0 ± 1.8 Hz, $n = 4$, $P = 0.02$; Supplemental Fig. S3*D* and *E*) and gain of ADP (from -1.4 ± 0.7 mV to 4.0 ± 2.3 mV, $n = 4$, $P = 0.06$; Supplemental Fig. S3*C* and *F*), similar to that seen following bath application of muscarine.

In conclusion, despite CCK-SCAs showing a biphasic hyperpolarization–depolarization change in V_m in response to muscarine, the increase in firing activity, adaptation coefficient, appearance of ADP and modulation of the APs width under mAChRs activation, strongly indicate that CCK+ interneurons (i.e. BCs and SCAs) share a common mechanism of mAChR modulation (Cea-del Rio *et al.* 2010).

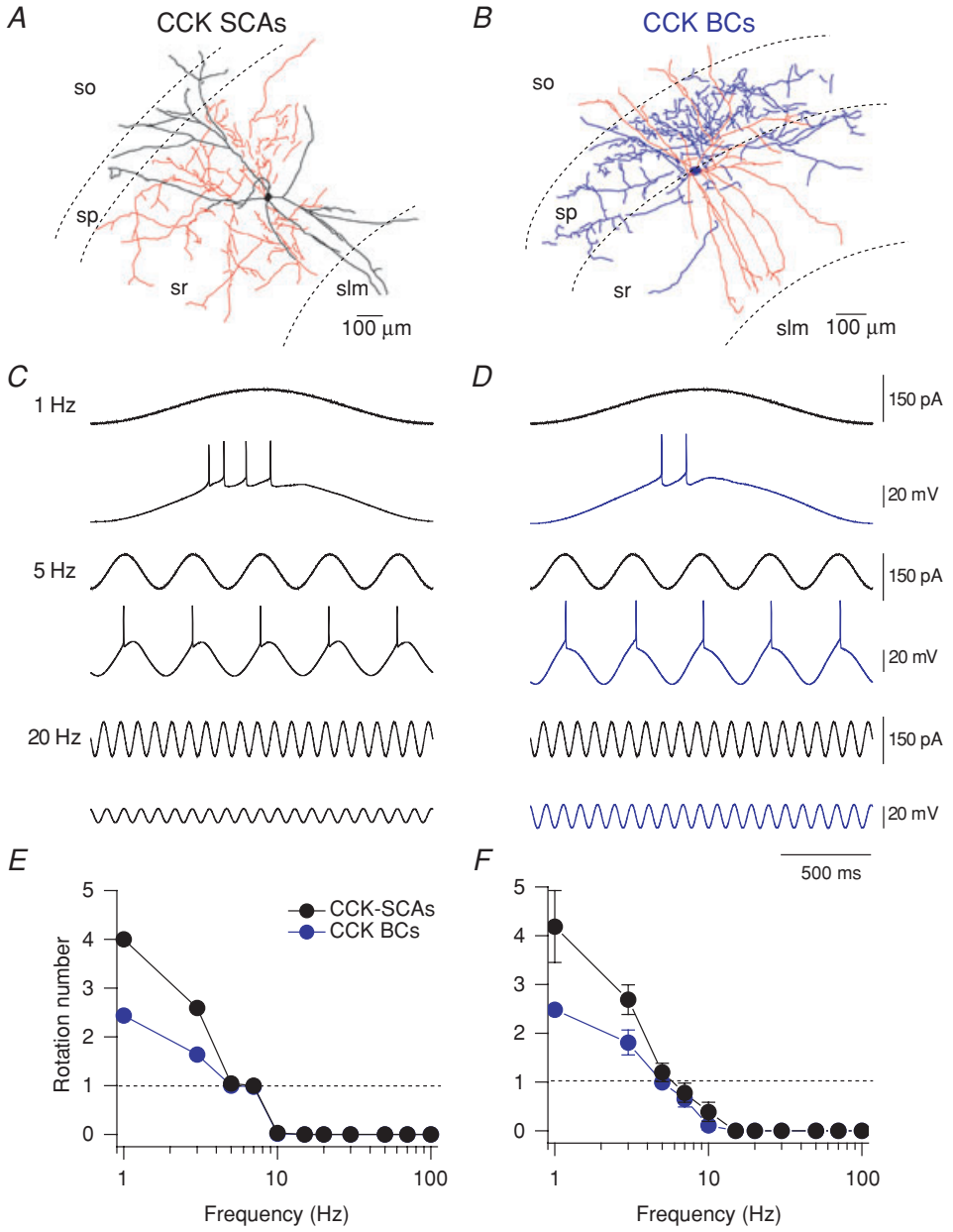

Figure 2. CCK-expressing interneurons generate action potentials during theta oscillatory activity
A and *B*, representative morphology pictures for CCK-SCAs and CCK-BCs. Phase-locked firing in response to sinusoidal current injections at 1, 5 and 20 Hz in CCK-SCAs (*C*) and CCK-BCs (*D*). *E*, rotation number (average AP per cycle) *versus* frequency for representative CCK-SCA (black circles) and CCK-BC (blue circles). *F*, rotation number (average AP per cycle) *versus* frequency for CCK-SCAs (black circles) and CCK-BCs (blue circles) populations.

M1 and M3 mAChRs control distinct aspects of mAChR-induced changes in CCK-SCA excitability

To explore what types of mAChRs are involved in the cholinergic response profile of CCK-SCAs we next used a combination of scRT-PCR and GAD65-GFP mice crossed with a number of mAChR knockout mice. To examine the mAChR mRNA present in CCK-SCAs, we first performed scRT-PCR for all mAChR subtypes (M1–M5) in a subset of nine CCK-SCAs. scRT-PCR revealed that 8/9 (92%) of CCK-SCAs expressed M1 mAChR mRNA, 17% expressed M2 mRNA, 58% expressed M3 mRNA, 75% expressed M4 mRNA and 50% expressed M5 mRNA (Fig. 4*A*).

M3 knockout mice (M3 KO) were then crossed with GAD65-GFP mice to permit recordings from identified CCK-SCAs lacking M3 mAChRs. Of the five M3 KO CCK-SCAs tested for scRT-PCR, all were negative for M3 mRNA receptor and M1 mRNA receptor was highly conserved similar to the wild type (80%; Fig. 4*B*). In CCK-SCAs recorded in M3 KO mice, both the mAChR-induced increase in firing frequency (Fig. 4*C* and *E*; from 13 ± 5 Hz to 12 ± 5 Hz, equivalent to 0.8 ± 0.1-fold, $n = 3$, $P = 0.4$) and the appearance of the mADP were eliminated (from -2.6 ± 0.9 mV to -0.5 ± 0.6 mV; $n = 3$; paired t test $P = 0.02$; Fig. 4*C* and *G*). Most interestingly, the biphasic response observed in the CCK-SCAs from WT mice shifted to a monotonic hyperpolarizing response in the CCK-SCAs in M3 KO mice (Fig. 4*H*; from -31.9 ± 9.4 pA to -19.6 ± 1.75, $n = 3$, $P = 0.045$), suggesting that the depolarization phase of the biphasic response in WT mice is mediated by M3 mAChRs.

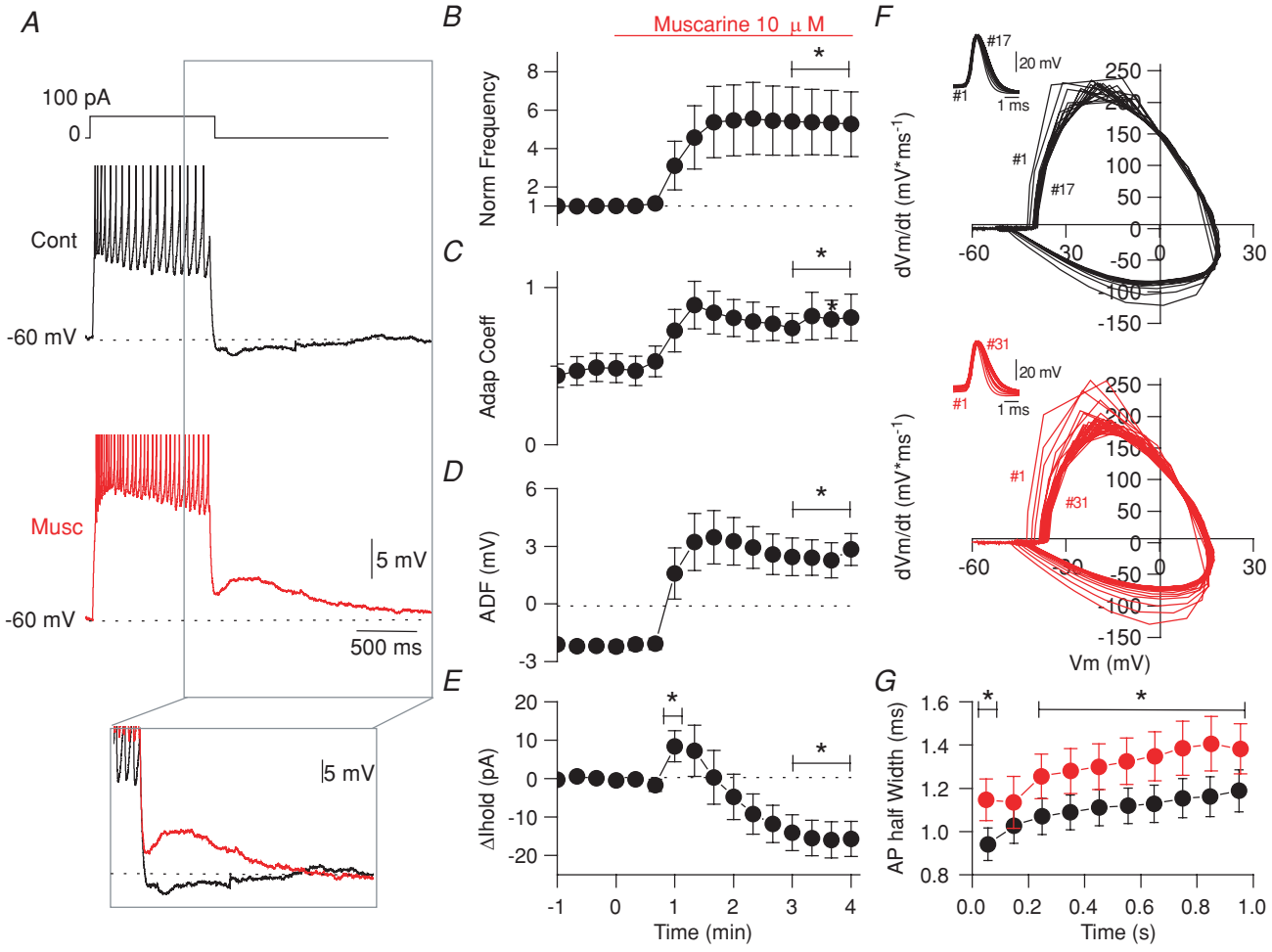

Figure 3. Cholinergic modulation of CCK-SCAs electrophysiological properties
A, voltage response from –60 mV in control (black) and after bath application of 10 μM muscarine (red) for CCK-SCAs. *B*, AP frequency normalized to the first minute. *C*, adaptation coefficient normalized to the first minute. *D*, afterdeflection (ADF) in a 200 ms window 200 ms after the current offset. *E*, ΔI_{hold} change relative to –60 mV holding potential. *F*, representative phase plots of d*V*/d*t* *versus* voltage of APs for CCK-SCAs in control conditions (black) and after bath application of 10 μM muscarine (red). *G*, AP half width, binned in 100 ms intervals during the 1 s current step for a population of 21 CCK-SCAs in control conditions (black) and after bath application of 10 μM muscarine (red).

In GAD65-GFP mice crossed with M1 KO mice, the mAChR-induced increase in firing frequency was reduced but still present in CCK-SCAs (2.6 ± 0.6-fold; from 9 ± 4 Hz to 19 ± 4 Hz, $n = 3$, $P = 0.0001$; Fig. 4*D* and , *E*). Second, as in M3 KO mice, the mAChR induced-ADP in CCK-SCAs was eliminated in M1 KO mice (Fig. 4*D* and *G*; from −2.0 ± 0.5 mV to −0.3 ± 0.8 mV, $n = 3$, $P = 0.05$). Strikingly, in CCK-SCAs lacking M1 mAChRs, the mAChR-induced change in holding current shifted in the opposite direction to that observed in M3 KO

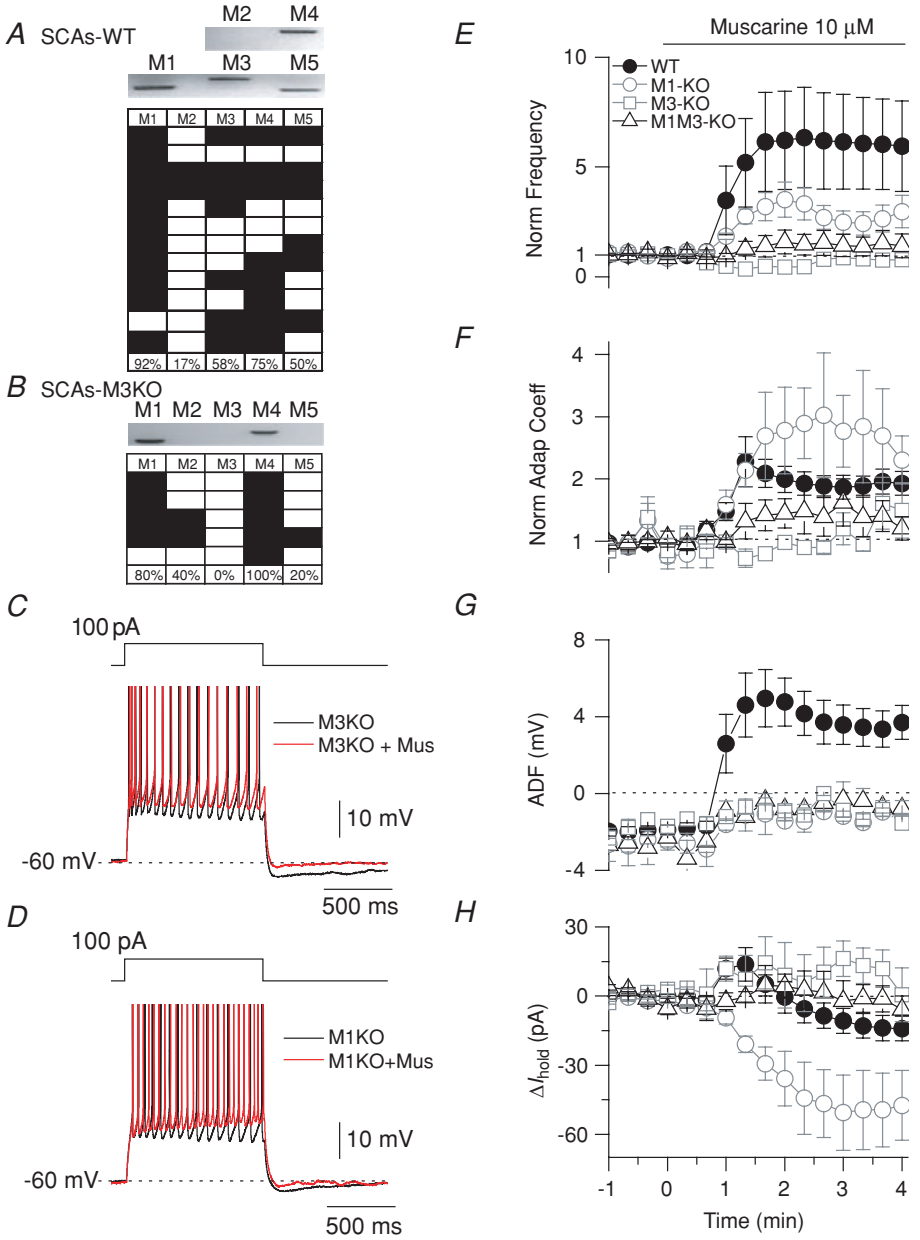

Figure 4. M1 and M3 muscarine receptors mediate the cholinergic phenotype of CCK-SCAs
A, representative scRT-PCR gel and mAChR profile for CCK-SCAs. *B,* scRT-PCR gel and mAChR profile for M3 KO CCK-SCAs. Representative traces for mAChR-induced changes in M3 KO CCK-SCAs (*C*) and M1 KO CCK-SCAs (*D*). *E*, normalized frequency summary population plot for control CCK-SCA (filled circles), M1 KO CCK-SCAs (open circles), M3 KO CCK-SCAs (open squares) and M1M3 KO CCK-SCAs (open triangles). *F*, normalized adaptation coefficient plot for control CCK-SCAs (filled circles), M1 KO CCK-SCAs (open circles), M3 KO CCK-SCAs (open squares) and M1M3 KO CCK-SCAs (open triangles). *G,* ADF summary population plot for control CCK-SCAs (filled circles), M1 KO CCK-SCAs (open circles), M3 KO CCK-SCAs (open squares) and M1M3 KO CCK-SCAs (open triangles). *H*, change in holding current for control CCK-SCAs (filled circles), M1 KO CCK-SCAs (open circles), M3 KO CCK-SCAs (open squares) and M1M3 KO CCK-SCAs (open triangles).

mice, shifting to a monophasic depolarizing response (from 2.5 ± 4.4 pA to -47.8 ± 16 pA, $n = 3$, unpaired t test $P = 0.02$; Fig. 4*H*).

Eliminating both M1 and M3 mAChRs from CCK-SCAs, achieved by crossing GAD65-GFP mice with the M1–M3 double KO mouse, blocked both the mAChR-induced increase in firing frequency (Fig. 4*E*; 14 ± 5 Hz to 12 ± 5 Hz, $n = 3$, $P = 0.4$) and prevented the emergence of the mADP (Fig. 4*G*; from -1.8 ± 0.5 mV to -1.2 ± 0.1, $n = 3$, $P = 0.4$). In addition, the biphasic changes in holding current observed in CCK-SCAs were completely abolished in the CCK-SCAs M1–M3 KO mice (Fig. 4*H*; from 0.7 ± 4.4 pA to -0.6 ± 6.4 pA, $n = 3$, $P = 0.7$ for the hyperpolarization response and from 0.7 ± 4.4 pA to -18 ± 10.1 pA, $n = 3$, $P = 0.7$ for the depolarization response). These data indicate that the cholinergic phenotype in CCK-SCAs can be completely accounted for by activation of both M1 and M3 mAChRs.

mAChR activation induces M3 mAChR-mediated subthreshold membrane potential oscillations in CCK$^+$ interneurons

Building on these data and the demonstration that CCK+ interneurons fire preferentially during theta oscillatory hippocampal activity (Klausberger & Somogyi, 2008), we next studied whether cholinergic modulation modified the oscillatory frequency preferences of both CCK-BCs and -SCAs by examining both spontaneous subthreshold membrane potential oscillations (MPOs) and their response to sinusoidal current injection during mAChR activation.

Subthreshold MPOs are rhythmic fluctuations of the resting V_m voltage which may facilitate firing activity at preferred oscillatory frequencies (Chapman & Lacaille, 1999). To determine the intrinsic oscillatory properties of CCK-SCAs and CCK-BCs, we analysed subtreshold oscillations at a holding potential close to rest (-60 mV). Under control conditions, both CCK-SCAs and CCK-BCs possessed a peak oscillatory power at frequencies in the delta range (1–2 Hz; CCK-SCAs: $8 \pm 2\ \mu V^{2*}Hz^{-1}$ and CCK-BCs: $14 \pm 2\ \mu V^{2*}Hz^{-1}$, Fig. 5*A*, *C*, *D* and *F*). Interestingly, the peak delta power of CCK-SCAs and CCK-BCs was enhanced at both depolarizing (-40 to -50 mV; CCK-SCAs: $230 \pm 78\ \mu V^{2*}Hz^{-1}$, $n = 7$, $P = 0.04$ and CCK-BCs: $33 \pm 13\ \mu V^{2*}Hz^{-1}$, $n = 36$, $P = 0.04$; Supplemental Fig. S4) and hyperpolarizing (-70 to -80 mV; CCK-SCAs: $84 \pm 24\ \mu V^{2*}Hz^{-1}$, $n = 14$, $P = 0.04$ and CCK-BCs: $36 \pm 8\ \mu V^{2*}Hz^{-1}$, $n = 33$, $P = 0.001$; Supplemental Fig. S4) membrane potentials. I_h conductances present in both SCAs (apparent upon sag; see Fig. 1*A*) and CCK BCs (Cea del Rio *et al.* 2010) may explain the increase in delta activity during hyperpolarizing membrane potentials. Depolarized membrane potentials revealed a secondary peak at theta frequencies (4–8 Hz). which is tightly related to the oscillatory engagement properties of both BCs and SCAs (Supplemental Fig. S4; CCK-SCAs: $176 \pm 69\ \mu V^{2*}Hz^{-1}$, $n = 7$, $P = 0.04$ and CCK-BCs: $19 \pm 9\ \mu V^{2*}Hz^{-1}$, $n = 36$, $P = 0.04$).

At a holding potential of -60 mV mAChR activation significantly increased the oscillatory power at delta frequencies in both CCK+ interneurons subtypes (CCK-SCAs: from $8 \pm 2\ \mu V^{2*}Hz^{-1}$ to $24 \pm 7\ \mu V^{2*}Hz^{-1}$, $n = 16$, $P = 0.04$ and CCK-BCs: from $14 \pm 2\ \mu V^{2*}Hz^{-1}$ to $6 \pm 1\ \mu V^{2*}Hz^{-1}$, $n = 29$, $P = 0.0006$, respectively; Fig. 5*A*, *C*, *D* and *F*). Neither CCK-lacking radiatum-projecting cells (from $13 \pm 5\ \mu V^{2*}Hz^{-1}$ to $16 \pm 6\ \mu V^{2*}Hz^{-1}$, $n = 5$, $P = 0.14$; Supplemental Fig. S5) nor PV-BCs (from $3 \pm 1\ \mu V^{2*}Hz^{-1}$ to $6 \pm 2\ \mu V^{2*}Hz^{-1}$, $n = 15$, $P = 0.12$; Supplemental Fig. S5) increased delta power in response to mAChR activation. These observations suggest that this mAChR-dependent amplification is preserved in CCK+ interneurons independent of their morphological characteristics.

To determine the mAChRs involved in amplifying intrinsic MPOs, we made recordings in M1 KO, M3 KO, and double M1–M3 KOs crossed with GAD65-GFP mice. When muscarine was applied to CCK+ M3 KO interneurons, neither CCK-SCAs (from $7 \pm 3\ \mu V^{2*}Hz^{-1}$ to $4 \pm 0.4\ \mu V^{2*}Hz^{-1}$, $n = 3$, $P = 0.5$; Fig. 5*B* and *C*) nor CCK-BCs (from $5 \pm 1\ \mu V^{2*}Hz^{-1}$ to $7 \pm 1\ V^{2*}Hz^{-1}$, $n = 9$, $P = 0.09$; Fig. 5*E* and *F*) exhibited an increase in delta frequency power. In contrast, mAChR-induced MPOs in CCK-SCAs (from $4 \pm 1\ \mu V^{2*}Hz^{-1}$ to $13 \pm 3\ \mu V^{2*}Hz^{-1}$, $n = 9$, $P = 0.03$; Fig. 5*C*) and CCK-BCs (from $3 \pm 1\ \mu V^{2*}Hz^{-1}$ to $13 \pm 3\ \mu V^{2*}Hz^{-1}$, $n = 3$, $P = 0.04$; Fig. 5*F*) were not abolished in M1 KO mice. Finally, as seen in M3 KO mice, mAChR-induced MPOs from both CCK-SCAs ($n = 3$, $P = 0.36$; Fig. 5*C*) and CCK-BCs ($n = 5$, $P = 0.1$; Fig. 5*F*) were completely abolished in M1–M3 KO mice. Taken together, these results indicate that cholinergic modulation of MPOs is controlled primarily by M3 mAChRs.

mAChR activation extends the frequency bandwidth preferences of CCK-BCs

To examine the impact of mAChR activation on the AP firing frequency preference of CCK-BCs and SCAs during oscillatory activity, muscarine (10 μM) was bath applied during sinusoidal current injection (frequency range 1–100 Hz) (as shown in control experiments described in Fig. 2). mAChR activation increased the phase-locking activity in both CCK+ cells at 1 Hz (Fig. 6) . However, mAChR activation enhanced the response to sinusoidal injection at 7 Hz in CCK-BCs (Fig. 6*D*), but not in

CCK-SCAs (Fig. 6*A*). To quantify the changes observed in CCK-SCAs and CCK-BCs, we examined R *versus* frequency in control and muscarine conditions (Fig. 6*B* and *E*). mAChR activation significantly increased R at delta and low-range theta frequencies in CCK+ cells (1–5 Hz; CCK-SCAs: from 2.7 ± 0.3 to 5.3 ± 0.5, $n = 3$, $P = 0.02$ and CCK-BCs: from 1.8 ± 0.2 to $6.6 \pm 0.0.5$, $n = 3$, $P = 0.003$). However, at frequencies greater than 7 Hz, R was not changed in CCK-SCAs (Fig. 6*A* and *E*; i.e. 7 Hz; from 0.78 ± 0.20 to 1.64 ± 0.28, $P = 0.1$), suggesting that the RC filtering characteristics and preferred frequency bandwidth was not changed from control conditions. We also examined the relationship between frequency and the incidence of AP failures (Fig. 6*C* and *F*). Failure probability plots showed that CCK-SCAs fired in each cycle from 1 to 5 Hz, and CCK-BCs fired without failure between 1 to 3 Hz (Fig. 6*C* and *F*). Both cell types steadily increased the AP failure

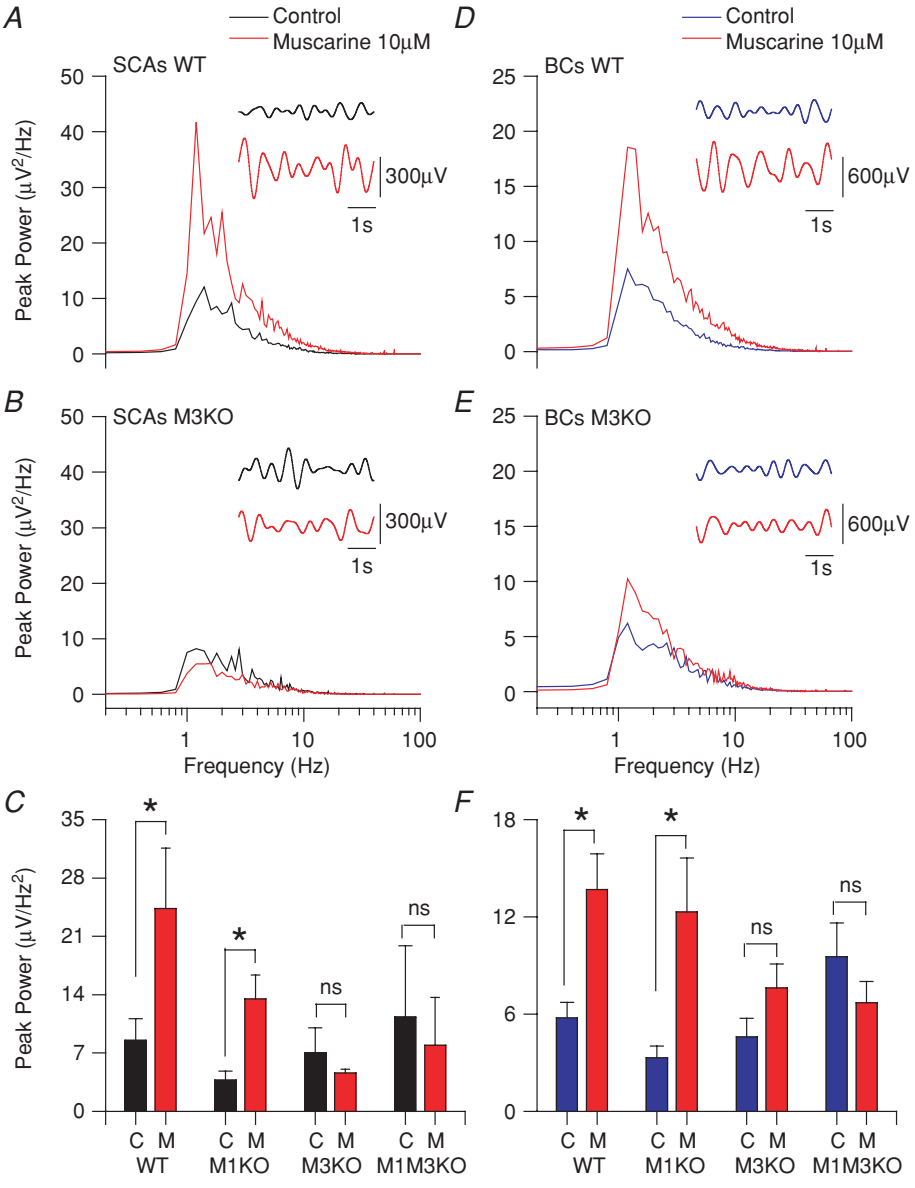

Figure 5. CCK-SCAs subthreshold oscillatory preferences
Power spectrum plot of subthreshold activity (holding V_m at −60 mV) for CCK-SCAs WT (*A*), M3 KO CCK-SCAs (*B*), WT CCK-BCs (*D*) and M3 KO CCK-BCs (*E*) population data in control conditions (black or blue trace) and muscarine 10 μM (red traces). The insets show 5 s holding resting potential raw traces filtered between 0.8 to 2.2 Hz in control (black or blue) and muscarine (red) conditions. *C*, bar plot of the CCK-SCAs population average data between 1 to 2 Hz for each condition. *F*, bar plot of the CCK-BCs population average data between 1 to 2 Hz for each condition.

rate until firing ceased at frequencies above 15 Hz. In CCK-BCs, bath application of muscarine caused a decrease in failure probability at frequencies between 10 and 20 Hz (15 Hz: from 1 ± 1 to 0.1 ± 0.06, $n = 3$, $P = 0.004$) that was more extended in bandwidth than CCK-SCAs (failure probability at 15 Hz: from 1 ± 1 to 0.9 ± 0.13, $n = 3$, $P = 0.37$). Finally, mAChR activation broadened the frequency bandwidth of CCK-BCs, extending R from theta into beta (7–20 Hz) frequencies (Fig. 6*F*; 15 Hz; 0.90 ± 0.06, $n = 3$, $P = 0.004$).

mAChR activation induces action potential phase precession and sharpens spike timing precision in CCK+ cells

To examine whether mAChR activation alters AP phase and spike time precision, we examined spiking timing of the first AP in the cycle at all frequencies tested. Raster plots of sinusoidal cycles at 7 Hz (Fig. 7*A*) and 10 Hz (Fig. 7*C*) from a representative CCK-SCA in control and in the presence of muscarine revealed that mAChR activation shifted AP firing to earlier in the cycle at 7 Hz (Fig. 7*B*), but

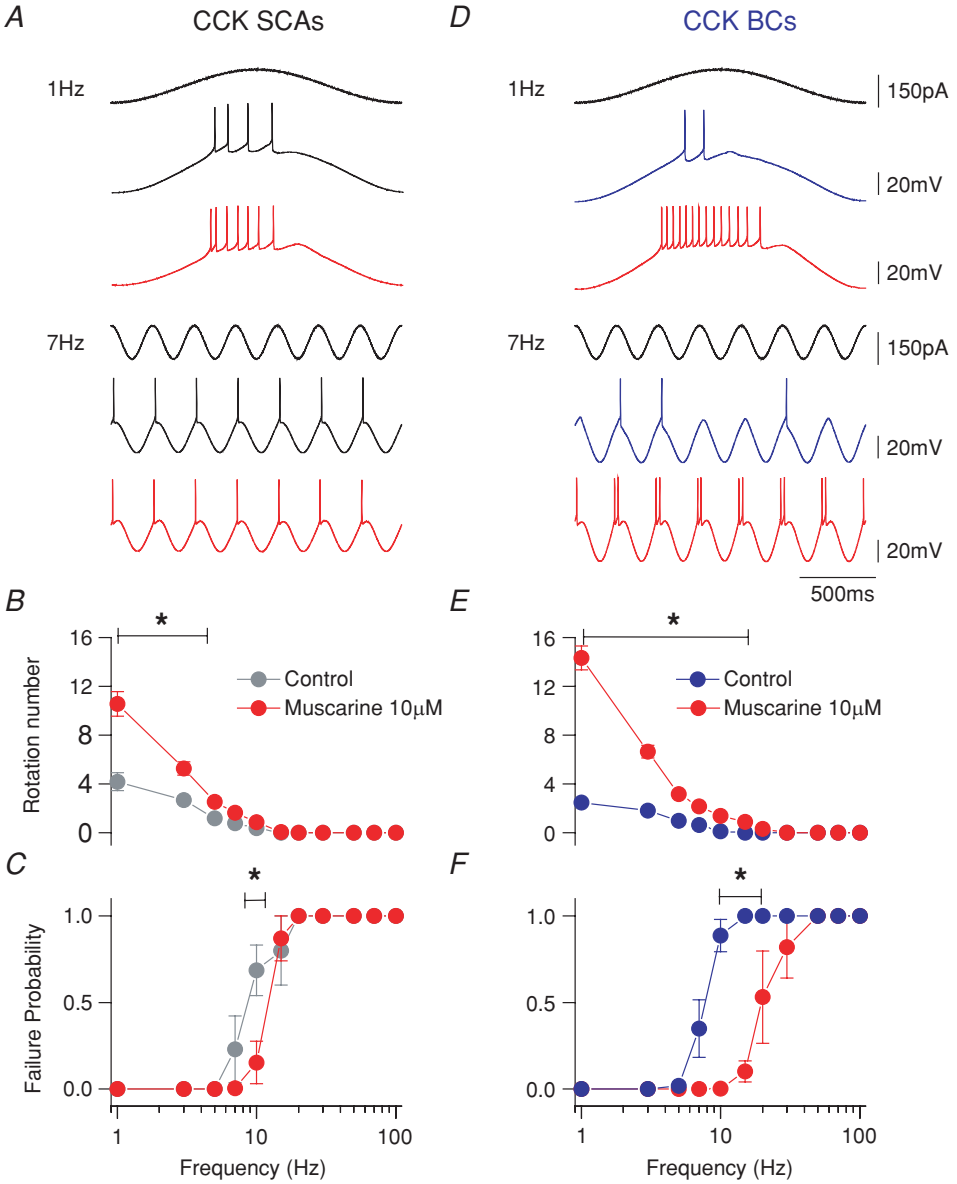

Figure 6. mAChR activation enhances AP generation to theta oscillatory activity in CCK-expressing cells and extends the sensitivity of CCK-BCs to beta frequency
A and *D*, representative traces at 1 and 7 Hz sinusoidal current injection for CCK-SCAs (black) and CCK-BCs (blue) in control conditions and after bath application of 10 μM muscarine (red). *B* and *E*, frequency *versus* rotation number (R) plot for SCA and BC interneuron populations. *C* and *F*, failure probability *versus* frequency populations plots for CCK-SCAs (black circles) and CCK-BCs in control (blue circles), and muscarine conditions (red circles).

not at 10 Hz (Fig. 7*D*). In a population of five CCK-SCAs, mAChR activation generated APs earlier in the cycle at 1–7 Hz (Fig. 7*E*; 7 Hz, 83.4 ± 3.6 deg *versus* 73.3 ± 1.5 deg, $n = 5$, $P = 0.04$) but was no longer significant at 10 Hz and above (Fig. 7*E*, 98.5 ± 7.3 deg *versus* 82.6 ± 3.2 deg, $n = 5$, $P = 0.08$). However, mAChR activation did not alter firing precision over the 1–10 Hz frequency band in the CCK-SCA population, as measured by jitter in the onset of AP firing during the cycle (Fig. 7*F*; 7 Hz: 0.2 ± 0.03 ms *versus* 0.2 ± 0.05 ms, $n = 5$, $P = 0.1$).

In contrast, mAChR activation of CCK-BCs was associated with a more reliable phase precession and increase in spike timing precision. Raster plots of sinusoidal cycles at 7 Hz (Fig. 8*A*) and 10 Hz (Fig. 8*C*) from a representative CCK-BC in control and in the presence of muscarine revealed that mAChR activation shifted AP firing to earlier in the cycle at 7 Hz (Fig. 8*B*) and 10 Hz (Fig. 8*D*). As a population, CCK-BCs shifted their AP firing phase earlier in the cycle at 7 Hz (7 Hz, 82.7 ± 1.8 deg *versus* 66.5 ± 2.2 deg, $n = 3$, $P = 0.04$; Fig. 8*E*) and at 10 Hz (87.6 ± 1.5 deg *versus* 70.6 ± 2.7 deg, $n = 3$, $P = 0.04$; Fig. 8*E*). Spike jitter in CCK-BCs did not change at lower frequencies but significantly decreased at 10 Hz (Fig. 8*B* and *F*; 0.5 ± 0.05 ms *versus* 0.08 ± 0.03 ms, $n = 5$, $P = 0.009$).

In summary, mAChR activation increased R at each frequency in both CCK-SCAs and CCK-BCs. However, in CCK-BCs mAChR activation was associated with a significant shift in their spike frequency preference, extending AP probability, phase locking and spike timing precision into the beta frequency range (15–20 Hz). Possibly due to their higher input resistance and limited

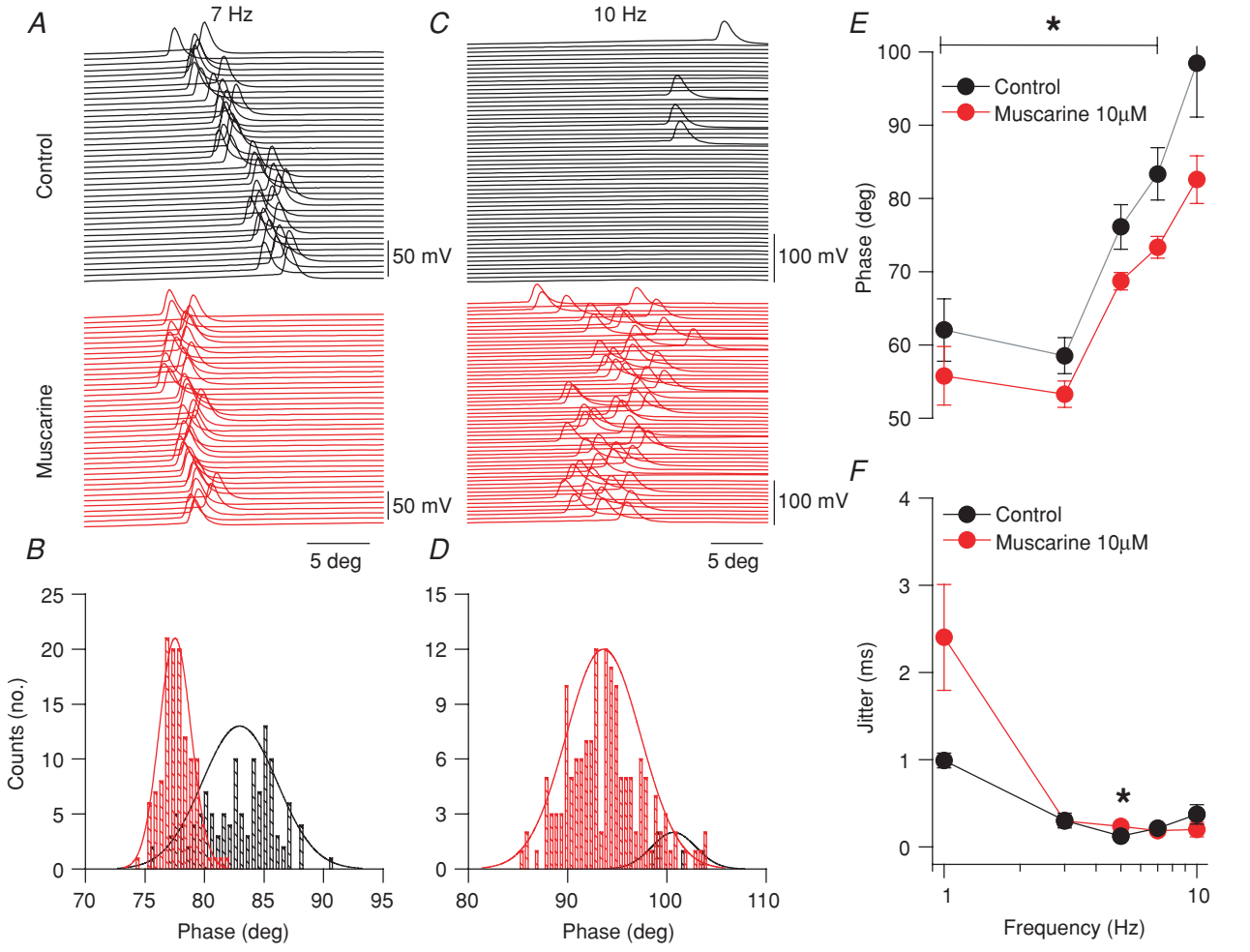

Figure 7. mAChRs activation reduces phase in CCK-SCAs
A, raster plots for spiking activity at 7 Hz sinusoidal current injections in control (black) and muscarine conditions (red). *B*, histogram of spike angle phase at 7 Hz sinusoidal current injection. *C*, raster plots for spiking activity at 10 Hz sinusoidal current injections in control (black) and muscarine conditions (red). *D*, histogram of spike angle phase at 10 Hz sinusoidal current injection. *E*, phase *versus* frequency plot for CCK-SCAs in control (black circles) and muscarine (red circles) conditions. *F*, jitter (S.D. of spike times) *versus* frequency plot for CCK-SCAs in control (black circles) and muscarine (red circles) conditions.

ability to follow higher input frequencies, mAChR activation in CCK-SCAs induced an increase in AP number (1–5 Hz) but not at high frequencies.

Discussion

In this study, we consistently identified CCK-containing SCAs using the GAD65-GFP mouse line in combination with scRT-PCR and electrophysiological experiments (Fig. 1*D*). CCK-SCAs undergo an increase in APs firing activity and the appearance of an ADP in response to mAChR activation, sharing a common response to that previously described for CCK-BCs (Cea-del Rio *et al.* 2010). However, in contrast to the muscarine-induced depolarization observed in CCK-BCs (Cea-del Rio *et al.* 2010), CCK-SCAs exhibited a biphasic response, which was initially hyperpolarizing then depolarizing in response. During this biphasic membrane potential change, M1 mAChRs govern the hyperpolarization while M3 mAChRs triggered the depolarization demonstrating a differential role for M1 and M3 mAChRs. We also examined the capacity of mAChR activation to alter spontaneous MPOs of CCK interneurons. Here, we showed for the first time that both CCK-SCAs and CCK-BCs possess high MPO activity at delta frequencies (1–2 Hz) under control conditions. Upon cholinergic modulation MPOs are amplified suggesting that CCK+ interneurons are responsive to muscarinic-driven oscillatory activity of the hippocampal network. MPOs were abolished in recordings from both CCK-BCs and CCK-SCAs in M3 KO mice, but remained intact in M1 KO mice. In experiments examining

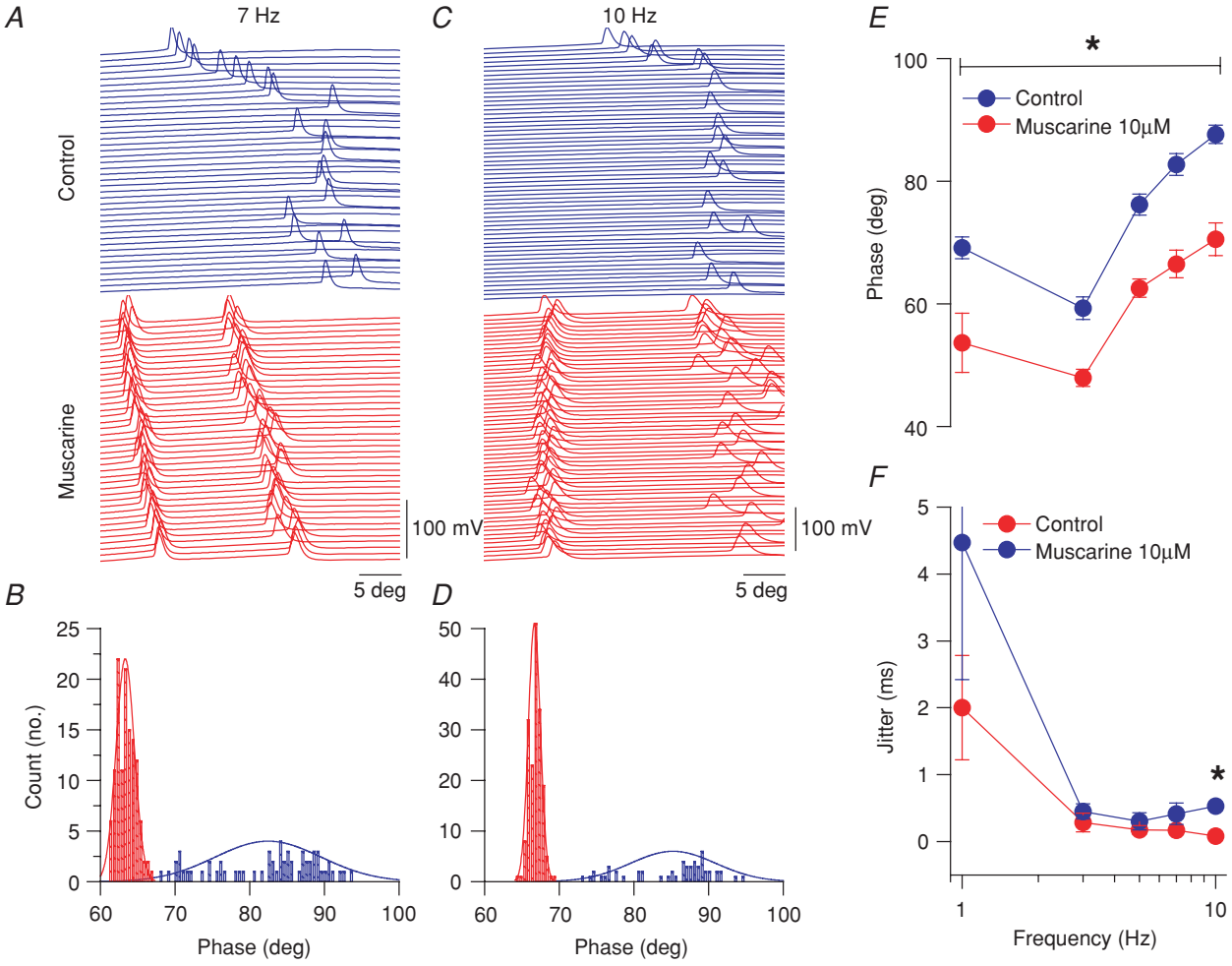

Figure 8. mAChRs activation reduces phase and sharpens spike timing precision at 10 Hz in CCK-BCs
A, raster plots for spiking activity at 7 Hz sinusoidal current injections in control (blue) and muscarine conditions (red). *B*, histogram of spike angle phase at 7 Hz sinusoidal current injection. *C*, raster plots for spking activity at 10 Hz sinusoidal current injections in control (blue) and muscarine conditions (red). *D*, histogram of spike angle phase at 10 Hz sinusoidal current injection. *E*, phase *versus* frequency plot for CCK-BCs in control (blue circles) and muscarine (red circles) conditions. *F*, jitter (S.D. of spike times) *versus* frequency plot for CCK-BCs in control (blue circles) and muscarine (red circles) conditions.

suprathreshold neuronal firing frequency preferences, CCK-SCAs fired preferentially in the delta/theta frequency range (1 to 7 Hz in CCK-SCAs and 1 to 5 Hz in CCK-BCs). which was amplified during cholinergic modulation, and may act to complement their intrinsic MPOs. However, although CCK-BCs exhibit a similar frequency preference as CCK-SCAs under control conditions, they shifted their frequency preference to beta oscillations following mAChR activation. This shift in frequency preference was also associated with phase precession during the whole range of frequencies tested (1 to 10 Hz) and enhanced spike timing precision at 10 Hz. Our results suggest that independent of somatodendritic morphology or axonal projection pattern, these two types of CCK-positive interneurons have somewhat stereotypic neuromodulatory properties that may allow them to function in a co-ordinate fashion during hippocampal network activity.

Potential mAChR subtype-specific mechanisms underlying the cholinergic phenotype of CCK-SCAs

We show that CCK-SCAs display changes in excitability and AP activity in response to mAChR activation similar to that observed in CCK-BCs (Cea-del Rio *et al.* 2010). Although CCK-SCAs and CCK-BCs show identical increases in excitability and AP firing frequency in response to mAChR activation (Fig. 2), the holding current changes required to maintain the cells at –60 mV were different between the two cell types. In contrast to the increase in holding current (corresponding to membrane depolarization) that CCK-BCs undergo (Cea-del Rio *et al.* 2010), CCK-SCAs showed a biphasic change corresponding to an initial hyperpolarization followed by depolarization of their membrane potential suggesting there may be a temporal window when somatic targeting interneurons are most active. This may act to dampen somatic excitability and to allow preferential input of dendritic excitation, only to then have both cells act concertedly. The hyperpolarization phase of the CCK-SCAs response was abolished in the M1 KO mice, whereas the depolarization phase was blocked in the M3 KO mice. In addition, M3 mAChRs primarily controlled changes in firing frequency whereas both M1 and M3 mAChRs controlled the emergence of the mADP (Fig. 4). This result suggests mAChR subtype-specific control of different intracellular signalling pathways and/or conductances are simultaneously activated on CCK-SCAs.

A likely candidate underlying the muscarinic-induced hyperpolarization phase of this biphasic response is the inwardly rectifying K^+ channel (GIRK). GIRK channels have been reported to underlie both the biphasic and hyperpolarizing responses in unidentified interneurons (McQuiston & Madison, 1999). Additionally, the M-current, a voltage-dependent potassium current mediated by Kv7 channels, is considered important for regulation of cell excitability by remaining active at voltage ranges close to AP initiation (Marrion, 1997; Lawrence *et al.* 2006*a*). In CCK-SCAs both the mAChR-induced increase in frequency firing and depolarization phase of the biphasic response was mediated by M3 mAChRs. Consistent with M3-mediated closure of the M-current, several studies using M1 mAChR KO mice failed to block the muscarinic-induced modulation of the M-current in CA1 pyramidal cells, indicating that another mAChR must be involved (Rouse *et al.* 2000; Fisahn *et al.* 2002). Thus, in contrast to CCK-BCs, where depolarizing influences predominate, our evidence suggests that mAChR-induced excitation of CCK-SCAs may arise through M3 mAChRs-mediated inhibition of the M-current preceded by an M1-mediated activation of GIRK channels.

mAChR activation also broadened the AP waveform in CCK-SCAs, suggesting that one or more potassium channels mediating AP repolarization may be inhibited by mAChR activation. CCK-positive interneurons with adaptive-firing patterns express Kv4.3 A-type potassium channels (Bourdeau *et al.* 2007), which are responsible for the regulation of firing frequency (Rudy, 1988) and shaping AP spike waveform (Zhang & McBain, 1995). Reduction of Kv4.3 channel-mediated current broadens the AP waveform of these cells (Bourdeau *et al.* 2007), suggesting that cholinergic modulation of CCK-SCAs APs may arise through the inhibition of Kv4.3 A-type potassium channels. Increased mAChR-induced broadening of the CCK-SCA AP also may be explained by the higher input resistance of CCK-SCAs that may accelerate the accumulation of Na^+ channel inactivation during repetitive firing. Future experiments will explore downstream effectors of mAChR-dependent modulation in these cell types.

Implications for hippocampal network processing

Cobb and colleagues observed that bulk fibre stimulation could induce atropine-sensitive biphasic responses onto dendritically projecting neurons, demonstrating that this complex response profile can be generated by synaptic activation of mAChRs (Widmer *et al.* 2006). Additionally, CCK+ interneurons participate in theta frequency oscillations (Klausberger *et al.* 2005; Tukker *et al.* 2007) and ablation of MS-DBB cholinergic neurons severely attenuates the magnitude of theta oscillations in the hippocampus (Lee *et al.* 1994). Taken together, these observations suggest a role for CCK interneurons in cholinergically induced theta oscillations.

Interneurons of stratum lacunosum moleculare assist in oscillatory network activity through cholinergic induction of intrinsic MPOs (Chapman & Lacaille, 1999). We show here that MPOs of both CCK-SCAs and CCK-BCs exhibit frequency preference at delta frequencies (1–2 Hz) and mAChR activation increases the power of these MPOs. Cholinergically induced MPOs and reduction in spike frequency adaptation are both abolished in CCK+ cells from M3 mAChR KO mice, suggesting that these phenomena may be mediated by the same M3 mAChR-sensitive conductances.

In experiments where sinusoidal currents were applied, both CCK-SCAs and CCK-BCs fired APs phase locked at frequencies equivalent to delta/theta activity (1–7 Hz). mAChR activation on both cell types amplified their activity at theta frequencies, but also shifted the CCK-BCs oscillatory engagement preference to higher beta frequencies (15–20 Hz). CCK-SCA somata and dendrites are aligned primarily with the Schaffer collateral/commissural input (Hajos & Mody, 1997; Vida *et al.* 1998; Gulyas *et al.* 1999*b*); therefore, they are poised to monitor the flow of activity from the CA3 region. Modulation of CCK-SCA excitability ultimately controls feed-forward inhibition onto pyramidal cell dendrites that may have consequences for synaptic integration at CA1 pyramidal cells dendrites. Although mAChR activation increases the excitability of both CCK-SCAs and CCK-BCs, mAChRs activation on CCK-SCAs does not result in a shift of their oscillatory engagement preferences to higher frequencies as seen with CCK-BCs. Instead CCK-SCAs simply amplify their AP firing activity preferences for theta frequency. Interestingly, CCK-positive interneurons possess a cholinergic receptor-induced mechanism of presynaptic inhibition (DSI) which is mediated by CB1-Rs (Freund & Katona, 2007; Neu *et al.* 2007). Despite their similar CB1-R densities, this mechanism is more powerful on perisomatic-targeting CCK-BCs than dendritic-targeting CCK-SCAs, when triggered either by tonic release of endocannabinoids or mGluR-driven endocannabinoid-mediated inhibition of GABA release (Lee *et al.* 2010). It is possible that mAChR activation of CCK-SCAs reduces feed-forward inhibition of CA1 pyramidal cell dendrites through CB1-R activation, allowing the propagation of gamma-modulated oscillatory activity in CA3 to spread into CA1.

In addition to the postsynaptic consequences of mAChR activation studied here, their presynaptic effects remain to be fully investigated. Recently, work of Hajos and colleagues demonstrated presynaptic inhibition through M2 mAChRs on PV-BC and axo-axonic terminals in the CA3 area of the hippocampus (Szabo *et al.* 2010). Interestingly, we detected M4 mAChR mRNA in a subset CCK-SCAs (Fig. 4), raising questions about the role of these potential presynaptic mAChRs in the CCK+ interneurons. Although evidence exists that M1–M4 heterodimers may mediate hyperpolarizing responses in neurons of the suprachiasmatic nucleus (Yang *et al.* 2010), the elimination of M1 receptors in SCAs largely accounts for the hyperpolarizing effect upon muscarine application. Although we cannot rule out a contribution of M4 receptors, M1 and M3 receptors appear to fully account for the depolarizing and hyperpolarizing responses of CCK-SCAs. Therefore, in order to understand the full impact of cholinergic modulation on inhibitory circuits, the full elucidation of the function of both presynaptic and postsynaptic mAChRs on BC and SCA subtypes remains to be clarified.

In conclusion, we demonstrate that neurochemically identical but morphologically distinct interneuronal populations are regulated by activation of mAChR subtypes in an equivalent fashion. CCK-SCAs and CCK-BCs share a cholinergic phenotype where the excitability and AP activity of these cells are increased, amplifying their activity at delta and theta frequencies in response to mAChRs activation. Thus, cholinergic input has the capacity to control CCK+ interneurons along the entire somato-dendritic axis.

References

Ascoli GA, Alonso-Nanclares L, Anderson SA, Barrionuevo G, Benavides-Piccione R, Burkhalter A *et al.* (2008). Petilla terminology: nomenclature of features of GABAergic interneurons of the cerebral cortex. *Nat Rev* **9**, 557–568.

Bergles DE, Doze VA, Madison DV & Smith SJ (1996). Excitatory actions of norepinephrine on multiple classes of hippocampal CA1 interneurons. *J Neurosci* **16**, 572–585.

Bourdeau ML, Morin F, Laurent CE, Azzi M & Lacaille JC (2007). Kv4.3-mediated A-type K^+ currents underlie rhythmic activity in hippocampal interneurons. *J Neurosci* **27**, 1942–1953.

Bragin A, Jando G, Nadasdy Z, Hetke J, Wise K & Buzsaki G (1995). Gamma (40–100 Hz) oscillation in the hippocampus of the behaving rat. *J Neurosci* **15**, 47–60.

Cauli B, Audinat E, Lambolez B, Angulo MC, Ropert N, Tsuzuki K, Hestrin S & Rossier J (1997). Molecular and physiological diversity of cortical nonpyramidal cells. *J Neurosci* **17**, 3894–3906.

Cea-del Rio CA, Lawrence JJ, Tricoire L, Erdelyi F, Szabo G & McBain CJ (2010). M3 muscarinic acetylcholine receptor expression confers differential cholinergic modulation to neurochemically distinct hippocampal basket cell subtypes. *J Neurosci* **30**, 6011–6024.

Chapman CA & Lacaille JC (1999). Intrinsic theta-frequency membrane potential oscillations in hippocampal CA1 interneurons of stratum lacunosum-moleculare. *J Neurophysiol* **81**, 1296–1307.

Cope DW, Maccaferri G, Marton LF, Roberts JD, Cobden PM & Somogyi P (2002). Cholecystokinin-immunopositive basket and Schaffer collateral-associated interneurones target different domains of pyramidal cells in the CA1 area of the rat hippocampus. *Neuroscience* **109**, 63–80.

Daw MI, Pelkey KA, Chittajallu R & McBain CJ (2010). Presynaptic kainate receptor activation preserves asynchronous GABA release despite the reduction in synchronous release from hippocampal cholecystokinin interneurons. *J Neurosci* **30**, 11202–11209.

Daw MI, Tricoire L, Erdelyi F, Szabo G & McBain CJ (2009). Asynchronous transmitter release from cholecystokinin-containing inhibitory interneurons is widespread and target-cell independent. *J Neurosci* **29**, 11112–11122.

Drummond GB (2009). Reporting ethical matters in *The Journal of Physiology*: standards and advice. *J Physiol* **587**, 713–719.

Fisahn A, Yamada M, Duttaroy A, Gan JW, Deng CX, McBain CJ & Wess J (2002). Muscarinic induction of hippocampal gamma oscillations requires coupling of the M1 receptor to two mixed cation currents. *Neuron* **33**, 615–624.

Foldy C, Lee SH, Morgan RJ & Soltesz I (2010). Regulation of fast-spiking basket cell synapses by the chloride channel ClC-2. *Nat Neurosci* **13**, 1047–1049.

Freund TF & Buzsaki G (1996). Interneurons of the hippocampus. *Hippocampus* **6**, 347–470.

Freund TF & Katona I (2007). Perisomatic inhibition. *Neuron* **56**, 33–42.

Garcia-Munoz A, Barrio LC & Buno W (1993). Membrane potential oscillations in CA1 hippocampal pyramidal neurons *in vitro*: intrinsic rhythms and fluctuations entrained by sinusoidal injected current. *Exp Brain Res* **97**, 325–333.

Glickfeld LL & Scanziani M (2006). Distinct timing in the activity of cannabinoid-sensitive and cannabinoid-insensitive basket cells. *Nat Neurosci* **9**, 807–815.

Gulyas AI, Acsady L & Freund TF (1999*a*). Structural basis of the cholinergic and serotonergic modulation of GABAergic neurons in the hippocampus. *Neurochem Int* **34**, 359–372.

Gulyas AI, Megias M, Emri Z & Freund TF (1999*b*). Total number and ratio of excitatory and inhibitory synapses converging onto single interneurons of different types in the CA1 area of the rat hippocampus. *J Neurosci* **19**, 10082–10097.

Hajos N & Mody I (1997). Synaptic communication among hippocampal interneurons: properties of spontaneous IPSCs in morphologically identified cells. *J Neurosci* **17**, 8427–8442.

Katona I, Sperlagh B, Sik A, Kafalvi A, Vizi ES, Mackie K & Freund TF (1999). Presynaptically located CB1 cannabinoid receptors regulate GABA release from axon terminals of specific hippocampal interneurons. *J Neurosci* **19**, 4544–4558.

Klausberger T, Marton LF, O'Neill J, Huck JH, Dalezios Y, Fuentealba P *et al.* (2005). Complementary roles of cholecystokinin- and parvalbumin-expressing GABAergic neurons in hippocampal network oscillations. *J Neurosci* **25**, 9782–9793.

Klausberger T & Somogyi P (2008). Neuronal diversity and temporal dynamics: the unity of hippocampal circuit operations. *Science* **321**, 53–57.

Kubota Y & Kawaguchi Y (1997). Two distinct subgroups of cholecystokinin-immunoreactive cortical interneurons. *Brain Res* **752**, 175–183.

Lambolez B, Audinat E, Bochet P, Crepel F & Rossier J (1992). AMPA receptor subunits expressed by single Purkinje cells. *Neuron* **9**, 247–258.

Lawrence JJ (2008). Cholinergic control of GABA release: emerging parallels between neocortex and hippocampus. *Trends Neurosci* **31**, 317–327.

Lawrence JJ, Saraga F, Churchill JF, Statland JM, Travis KE, Skinner FK & McBain CJ (2006*a*). Somatodendritic Kv7/KCNQ/M channels control interspike interval in hippocampal interneurons. *J Neurosci* **26**, 12325–12338.

Lawrence JJ, Statland JM, Grinspan ZM & McBain CJ (2006*b*). Cell type-specific dependence of muscarinic signalling in mouse hippocampal stratum oriens interneurones. *J Physiol* **570**, 595–610.

Lee MG, Chrobak JJ, Sik A, Wiley RG & Buzsaki G (1994). Hippocampal theta activity following selective lesion of the septal cholinergic system. *Neuroscience* **62,** 1033–1047.

Lee SH, Foldy C & Soltesz I (2010). Distinct endocannabinoid control of GABA release at perisomatic and dendritic synapses in the hippocampus. *J Neurosci* **30**, 7993–8000.

Leung LS & Yu HW (1998). Theta-frequency resonance in hippocampal CA1 neurons in vitro demonstrated by sinusoidal current injection. *J Neurophysiol* **79**, 1592–1596.

Lopez-Bendito G, Sturgess K, Erdelyi F, Szabo G, Molnar Z & Paulsen O (2004). Preferential origin and layer destination of GAD65-GFP cortical interneurons. *Cereb Cortex* **14**, 1122–1133.

McQuiston AR & Madison DV (1999). Muscarinic receptor activity has multiple effects on the resting membrane potentials of CA1 hippocampal interneurons. *J Neurosci* **19**, 5693–5702.

Marrion NV (1997). Control of M-current. *Annu Rev Physiol* **59**, 483–504.

Miles R, Toth K, Gulyas AI, Hajos N & Freund TF (1996). Differences between somatic and dendritic inhibition in the hippocampus. *Neuron* **16**, 815–823.

Neu A, Foldy C & Soltesz I (2007). Postsynaptic origin of CB1-dependent tonic inhibition of GABA release at cholecystokinin-positive basket cell to pyramidal cell synapses in the CA1 region of the rat hippocampus. *J Physiol* **578**, 233–247.

Parra P, Gulyas AI & Miles R (1998). How many subtypes of inhibitory cells in the hippocampus? *Neuron* **20**, 983–993.

Pike FG, Goddard RS, Suckling JM, Ganter P, Kasthuri N & Paulsen O (2000). Distinct frequency preferences of different types of rat hippocampal neurones in response to oscillatory input currents. *J Physiol* **529**, 205–213.

Pouille F & Scanziani M (2001). Enforcement of temporal fidelity in pyramidal cells by somatic feed-forward inhibition. *Science* **293**, 1159–1163.

Rouse ST, Hamilton SE, Potter LT, Nathanson NM & Conn PJ (2000). Muscarinic-induced modulation of potassium conductances is unchanged in mouse hippocampal pyramidal cells that lack functional M1 receptors. *Neurosci Lett* **278**, 61–64.

Rudy B (1988). Diversity and ubiquity of K channels. *Neuroscience* **25**, 729–749.

Szabo GG, Holderith N, Gulyas AI, Freund TF & Hajos N (2010). Distinct synaptic properties of perisomatic inhibitory cell types and their different modulation by cholinergic receptor activation in the CA3 region of the mouse hippocampus. *Eur J Neurosci* **31**, 2234–2246.

Tukker JJ, Fuentealba P, Hartwich K, Somogyi P & Klausberger T (2007). Cell type-specific tuning of hippocampal interneuron firing during gamma oscillations *in vivo*. *J Neurosci* **27,** 8184–8189.

Vida I, Halasy K, Szinyei C, Somogyi P & Buhl EH (1998). Unitary IPSPs evoked by interneurons at the stratum radiatum-stratum lacunosum-moleculare border in the CA1 area of the rat hippocampus *in vitro*. *J Physiol* **506**, 755–773.

Widmer H, Ferrigan L, Davies CH & Cobb SR (2006). Evoked slow muscarinic acetylcholinergic synaptic potentials in rat hippocampal interneurons. *Hippocampus* **16**, 617–628.

Yang JJ, Wang YT, Cheng PC, Kuo YJ & Huang RC (2010). Cholinergic modulation of neuronal excitability in the rat suprachiasmatic nucleus. *J Neurophysiol* **103**, 1397–1409.

Zhang L & McBain CJ (1995). Potassium conductances underlying repolarization and after-hyperpolarization in rat CA1 hippocampal interneurones. *J Physiol* **488**, 661–672.

Author contributions

C.A.C.-d.R., J.J.L. and C.J.McB. designed the experiments and research; C.A.C.-dR. performed the research; C.A.C.-dR. and J.J.L. analysed the data; F.E. and G.S. generated the GAD65-GFP transgenic mice; C.A.C.-dR., J.J.L.and C.J.McB. wrote the paper. All the experiments were performed in the Eunice Kennedy Shriver NICHD at the NIH. All authors read and approved the manuscript for publication.

Acknowledgements

NICHD intramural funding (C.J.McB.) supported this work. We are grateful to Drs Bruno Cauli for primers, Jurgen Wess for all muscarinic acetylcholine receptor knockout mice, Ludovic Tricoire for the training in the scRT-PCR technique, Jordan Pauli and David Bonislawski for the processing and imaging acquisition of the GAD65-GFP/Neurotrace and GAD65-GFP/vAChT slice picture in Supplemental Fig S3, and Vincent Schram and the NICHD Microscopy and Imaging Core for assisting in the acquisition of tiled 3D confocal images of biocytin-labelled cells. C.A.C.-dR. was a doctoral student from the graduate program partnership between NIH and the CNIV of the University of Valparaíso, Chile. We finally thank Brian Jeffries for immunocytochemistry, biocytin labelling and morphological drawings, and members of the McBain and Lawrence laboratories for helpful comments on the manuscript.